Science Advances
AAAS

Supplementary Materials for

FGF21 modulates mitochondrial stress response in cardiomyocytes only under mild mitochondrial dysfunction

Marijana Croon*, Karolina Szczepanowska, Milica Popovic, Christina Lienkamp, Katharina Senft, Christoph Paul Brandscheid, Theresa Bock, Leoni Gnatzy-Feik, Artem Ashurov, Richard James Acton, Harshita Kaul, Claire Pujol, Stephan Rosenkranz, Marcus Krüger, Aleksandra Trifunovic*

*Corresponding author. Email: aleksandra.trifunovic@uk-koeln.de (A.T.); maradjan@uni-koeln.de (M.K.)

Published 6 April 2022, *Sci. Adv.* **8**, eabn7105 (2022)
DOI: 10.1126/sciadv.abn7105

This PDF file includes:

Other Supplementary Material for this manuscript includes the following:

Material and Methods

Antibodies

Mouse monoclonal anti-ATP5A	Abcam	Cat#ab14748
Mouse monoclonal anti-COX4	Molecular Probes	Cat #A21348
Mouse monoclonal anti - GAPDH	Abcam	ab9484
Mouse monoclonal anti-GRP75	Abcam	ab82591
Mouse monoclonal anti-HSC70	Santa Cruz	Cat#sc7298
Mouse monoclonal anti-HSP60	BD	611562
Mouse monoclonal anti-LONP1	Abcam	Cat# ab82591,
Mouse monoclonal anti-MT-CO1	Molecular Probes	Cat #459600
Mouse monoclonal anti-MTHFD2	Abcam	ab56772
Mouse monoclonal anti-NDUFA9	Molecular Probes	Cat#459100
Mouse monoclonal anti-NDUFB6	Invitrogen	Cat#A21359
Mouse monoclonal anti- NDUFS4	Abcam	ab87399
Mouse monoclonal anti-SDHA	Molecular Probes	Cat#459200
Mouse monoclonal anti-OXPHOS cocktail (ATP5A, UQCRC2, COX1, SDHB, NDUFB8)	Abcam	ab110413
Mouse monoclonal anti-p62	Abnova	H00008878-M01
Mouse monoclonal anti-UQCRC1	Molecular Probes	Cat#459140
Mouse monoclonal anti-UQCRFS1/RISP [5A5]	Abcam	Cat#ab14746
Goat polyclonal anti-Klotho β	R&D Systems	AF2619
Rabbit polyclonal anti-ATF4 (CREB-2)	Santa Cruz	Sc-200
Rabbit polyclonal 4E-BP1	CST	#4923
Rabbit polyclonal 4E-BP1 (phospho Thr37/46)	CST	#2855
Rabbit polyclonal anti-AFG3L2	Elena Rugarli, Uni. Cologne	N/A
Rabbit polyclonal anti-BECLIN-1	CST	3738
Rabbit polyclonal anti-Calnexin (CANX)	Calbiochem	208880
Rabbit polyclonal anti-CLPP	Sigma	Cat#HPA040262
Rabbit polyclonal anti-eIF2a	Abcam	ab26197
Rabbit monoclonal anti-EIF2a (phospho S51)	Abcam	ab32157
Rabbit monoclonal anti ERK1/2 (phospho hr202/Tyr204)	CST	#9101
Rabbit polyclonal anti-LC3B	CST	#2775
Rabbit polyclonal anti-LONP1	Abcam	ab103809
Rabbit polyclonal anti-MTHFD1L	Proteintech	16113-1-AP
Rabbit polyclonal anti-NDUFS2	Abcam	ab96160

Rabbit polyclonal anti-NDUFV2	Proteintech	15301-1-AP
Rabbit polyclonal anti-PRAS40	CST	#2610
Rabbit polyclonal anti-PRAS40 (Phospho T246)	CST	#2997
Rabbit polyclonal anti-PYCR1	Abcam	ab94780
Rabbit polyclonal anti-P5CS (ALDH18A1)	Proteintech	17719-1-AP
Rabbit polyclonal anti-SHMT2	Abcam	ab224428
Rabbit polyclonal anti-TFAM	Courtesy of N.Larsson's Lab	N/A

qPCR Primers

mAtf4 F (5' AACATCCAATCTGTCCCGG 3')	This paper
mAtf4 R (5' GTTCTCCAGCGACAAGGC 3')	This paper
mNppa F (5' ATGGGCTCCTTCTCCATCA 3')	This paper
mNppa R (5' CCTGCTTCCTCAGTCTGCTC 3')	This paper
mNppb F (5' GGATCTCCTGAAGGTGCTGT 3')	This paper
mNppb R (5' TTCTTTTGTGAGGCCTTGGT 3')	This paper
mFgf21 F (5' GTGTCAAAGCCTCTAGGTTTCTT 3')	*(13)*
mFgf21 R (5' GGTACACATTGTAACCGTCCTC 3')	*(13)*
mFgfr1 F (5' TATGTCCAGATCCTGAAGAC 3')	This paper
mFgfr1 R (5' GAGAGTCCGATAGAGTTACC 3')	This paper
mKlb F (5' CTAAACCAGGTTCTTCAAGC 3')	This paper
mKlb R (5' GATCTGCTTGTAGTAATGAGC 3')	This paper
mSirt1 F (5' GCAGGTTGCAGGAATCCAA 3')	This paper
mSirt1 R (5' GGCAAGATGCTGTTGCAAA 3')	This paper
mPpara F (5' AACATCGAGTGTCGAATATGTGG *3')*	This paper
mPpara R (5' CCGAATAGTTCGCCGAAAGAA 3')	This paper
mUcp1 F (5' AGCCATCTGCATGGGATCAAA 3')	*(13)*
mUcp1 R (5' GGGTCGTCCCTTTCCAAAGTG *3')*	*(13)*
mDio2 F (5' CAGCTTCCTCCTAGATGCCTA *3')*	*(13)*
mDio2 R (5' CTGATTCAGGATTGGAGACGTG *3')*	*(13)*
mCidea F (5' TGACATTCATGGGATTGCAGAC 3')	*(13)*
mCidea R (5' GGCCAGTTGTGATGACTAAGAC 3')	*(13)*
mFgf19 F (5' CCAGAGAACAGCTCCAGGAC *3')*	This paper
mFgf19 R (5' TCCATGCTGTCACTCTCCAG *3')*	This paper
mFgf23 F (5' TGGGCACTGCTAGAGCCTAT *3')*	This paper
mFgf23 R (5' CTTCGAGTCATGGCTCCTGT *3')*	This paper
mGrp78 F (5' TGGTGAGCGACTTGTTGGAAT 3')	This paper
mGrp78 R (5' ATTGGAGGCACGGACAATTTT *3')*	This paper
mPsat1 F (5' AGTGGAGCGCCAGAATAGAA 3')	This paper
mPsat1 R (5' AGTGGAGCGCCAGAATAGAA *3')*	This paper
mPhghd F (5' GACCCCATCATCTCTCCTGA *3')*	This paper
mPhghd R (5' GCACACCTTTCTTGCACTGA *3')*	This paper
mLonp1 F (5' ATGACCGTCCCGGATGTGT 3')	This paper
mLonp1 R (5' CCTCCACGATCTTGATAAAGCG 3')	This paper

mAfg3l2 F (5' GTTGATGGGCAATACGTCTGG 3')	This paper
mAfg3l2 R (5' GACCCGGTTCTCCCCTTCT *3')*	This paper
mHsp60 F (5' GCCTTAATGCTTCAAGGTGTAGA *3')*	This paper
mHsp60 R (5' CCCCATCTTTTGTTACTTTGGGA *3')*	This paper
mShmt2 F (5' CCACCACCACTCACAAGACACTGCG3')	This paper
mShmt2 R (5' TGTAGGGATGG GAACACAGCGAAGTTG 3')	This paper
mPycr1 F (5'GATGCTCTGGCTGACGGTGGTGT 3')	This paper
mPycr1 R (5'GCTGGCTGGGATGCTGTTCTGAG 3')	This paper
mMthfd2 F (5' CCACTCCCAGAGCACATTGAT 3')	This paper
mMthfd2 R (5' GTTGGAATGCCTGTTCGCTT 3')	This paper
mChop10 F (5' CTGGAAGCCTGGTATGAGGAT 3')	This paper
mChop10 R(5' CAGGGTCAAGAGTAGTGAAGGT 3')	This paper
mAldh18a1 F (5' AATCAGGGCCGAGAGATGATG 3')	This paper
mAldh18a1 R (5' GGCCTCTAAGACCGGAATTGC 3')	This paper
mcMyc F (5' AGCCCCTAGTGCTGCATGA *3')*	This paper

Label-free quantification of the cardiac proteome

Mass spectrometry: The samples were further processed using a 'Q Exactive Plus Orbitrap' (Thermo Fisher Scientific) mass spectrometer coupled with an 'EASY nLC' (Thermo Fisher Scientific). An in-house packed analytical column (50 cm — 75 µm I.D., filled with 2.7 µm Poroshell EC120 C18, Agilent) was used to load the samples with solvent A (0.1% formic acid in water). Chromatographic separation was performed at a constant flow rate of 250 nL/min using the following gradient: 5-28% solvent B (0.1% formic acid in 80 % acetonitrile) within 220.0 min, 28-55% solvent B within 5.0 min, 55-90% solvent B within 5.0 min, followed by washing and column equilibration. The mass spectrometer was operated in data-dependent acquisition mode. The MS1 survey scan was acquired from 300-1750 m/z at a resolution of 70,000. The top 10 most abundant peptides were isolated within a 2.1h window and subjected to HCD fragmentation at a normalized collision energy of 27%. The AGC target was set to 5e5 charges, allowing a maximum injection time of 60 ms. Product ions were detected in the Orbitrap at a resolution of 17,500. Precursors were dynamically excluded for 20s.

The generated mass-spectrometry (MS) raw data were analyzed using MaxQuant analysis software and the implemented Andromeda software . Peptides and proteins were identified using the mouse UniProt trembl database (downloaded 08/2019) with common contaminants. All parameters in MaxQuant were set to the default values. Trypsin was selected as the digestion enzyme, and a maximum of two missed cleavages was allowed.

Methionine oxidation and N-terminal acetylation were set as variable modifications, and carbamidomethylation of cysteines was chosen as a fixed modification. The label-free quantification (LFQ) algorithm was used to quantify the measured peptides and the "match between runs" option was enabled to quantify peptides with a missing MS_2 spectrum.

Subsequent statistical analysis was performed using Perseus (1.6.10.50) software. Potential contaminants and reverse peptides were excluded, and values were log_2 transformed. Welch's Student *t*-test with S_0=0.1 and a permutation-based FDR of 0.05 or 0.01 with 500 randomizations was performed to obtain differentially regulated proteins between the two groups. Identified proteins were annotated with the following Gene Ontology terms: Biological Process, Molecular Function, and Cellular Compartment, and the Reactome Pathway database. Finally, graphical visualization was achieved using Instant Clue software.

RNA sequencing (RNAseq) of cardiac total mRNA

Adapter and read quality trimming was performed with fastp v0.21.0 *(59)* ,psuedo-alignment to The Mus Musculus genome (GRCm38.p6 Ensembl Release 97) was performed with Kallisto v0.46.1 *(60)* and differential gene expresion analysis was performed in R v4.0.3 (2021-08-10) (R Core Team. 2021. *R: A Language and Environment for Statistical Computing*. Vienna, Austria: R Foundation for Statistical Computing. https://www.R-project.org/.) with EdgeR v3.32.1 *(61)*.

Raw counts were read with tximport v1.18.0 *(62)* and subject to variance stabalising transformation (VST) using DESeq2 v1.30.1 *(63)* for the purposes of plotting expression levels.

Figure S1

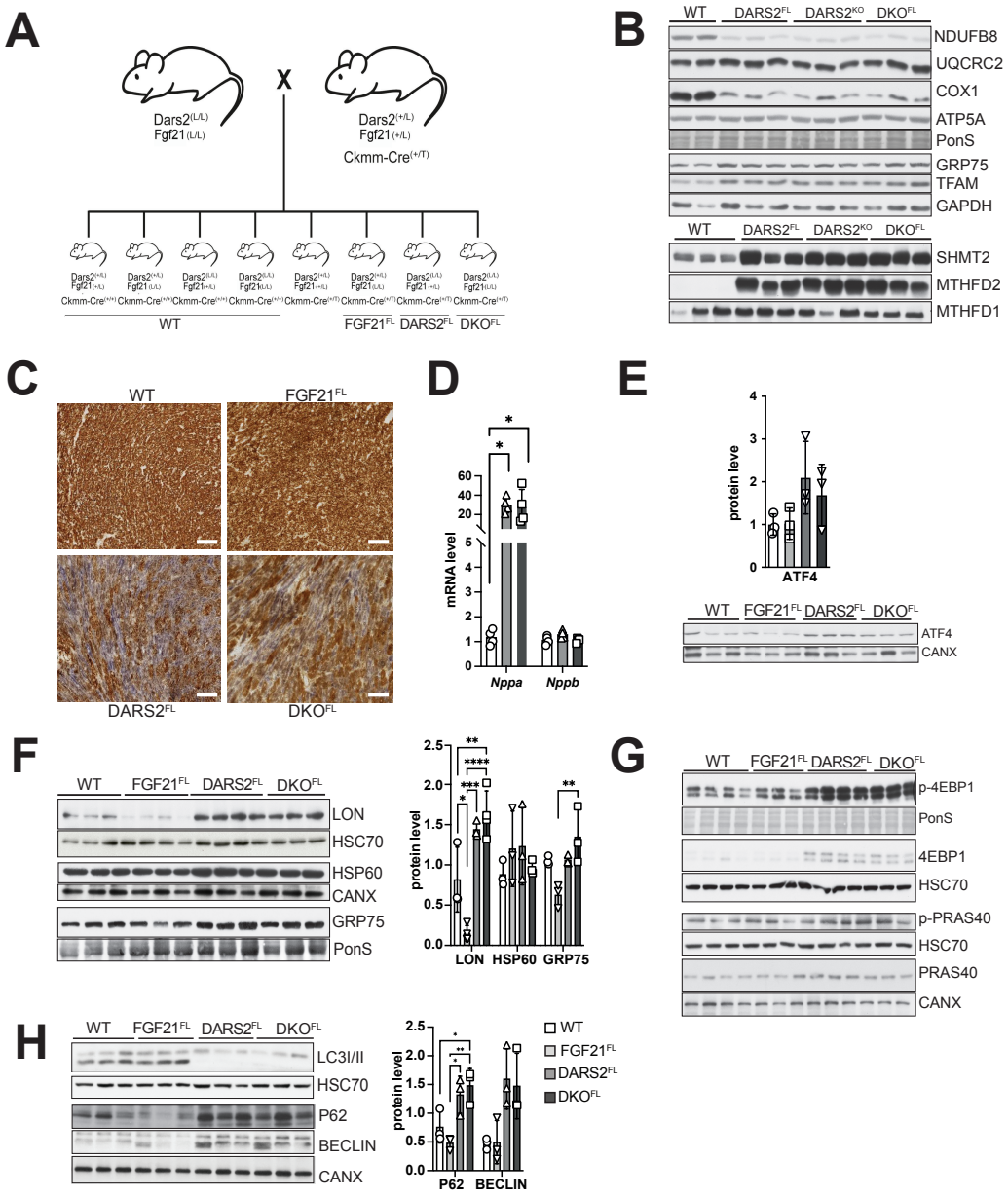
A
Dars2(L/L) Fgf21(L/L)
X
Dars2(+/L) Fgf21(+/L) Ckmm-Cre(+/T)
WT
FGF21FL DARS2FL DKOFL
B
WT DARS2FL DARS2KO DKOFL
NDUFB8
UQCRC2
COX1
ATP5A
PonS
GRP75
TFAM
GAPDH
SHMT2
MTHFD2
MTHFD1
C
WT
FGF21FL
DARS2FL
DKOFL
D
mRNA level
Nppa
Nppb
E
protein leve
ATF4
ATF4
CANX
F
LON
HSC70
HSP60
CANX
GRP75
PonS
protein level
LON HSP60 GRP75
G
p-4EBP1
PonS
4EBP1
HSC70
p-PRAS40
HSC70
PRAS40
CANX
H
LC3I/II
HSC70
P62
BECLIN
CANX
protein level
P62 BECLIN

Figure S1. Tissue-specific loss of FGF21 in DARS2 does not additionally exacerbate stress responses.

(A) Breeding scheme for generation of wild type (WT), $FGF21^{FL}$, $DARS2^{FL}$ and DKO^{FL} mice. Allele nomenclature: wild type (+), transgene (tg), floxed (L). $DARS2^{FL}$, $FGF21^{FL}$ or DKO^{FL} stand for specific depletion of DARS2, FGF21 or both under Ckmm-Cre promoter in heart and skeletal muscle. $DARS2^{FL}$ carries also a heterozygous FGF21 depletion, while $DARS2^{KO}$ does not. (B) Western blot analysis of steady-state levels of proteins in cardiac lysates of 6-week-old WT, $DARS2^{FL}$, $DARS2^{KO}$ and DKO^{FL} mice. Antibodies used were raised against protein indicated in the panel. HSC70 was used as loading control (n=3). (C) Enzymatic cytochrome c oxidase/ succinate dehydrogenase (COX/SDH) staining; scale bars: 50µm (n=3). (D) Relative transcript levels of *Nppa* and *Nppb* cardiomyopathy markers determined by RT-qPCR (n=3-4). (E) Western blot analysis and quantification of ATF4 protein levels in heart lysates of 6-week-old mice. CANX was used as a loading control (n=3). (F) Western blot and quantification of UPR^{mt} markers in 6-week-old hearts. HSC70 and CANX were used as loading controls (n=3). (G) Western blot analyses of proteins involved in mTOR pathway in 6-week-old hearts. HSC70, PonS and CANX were used as loading controls (n=3). (H) Western blot and quantification of markers of autophagy in 6-week-old hearts. HSC70 and CANX were used as loading controls (n=3). (D, E, F and H) Bars represent mean ± SD (one-way ANOVA and Tukey's multiple comparisons test, *$p<0.05$, **$p<0.01$, ***$p<0.001$, ****$p<0.0001$).

Figure S2

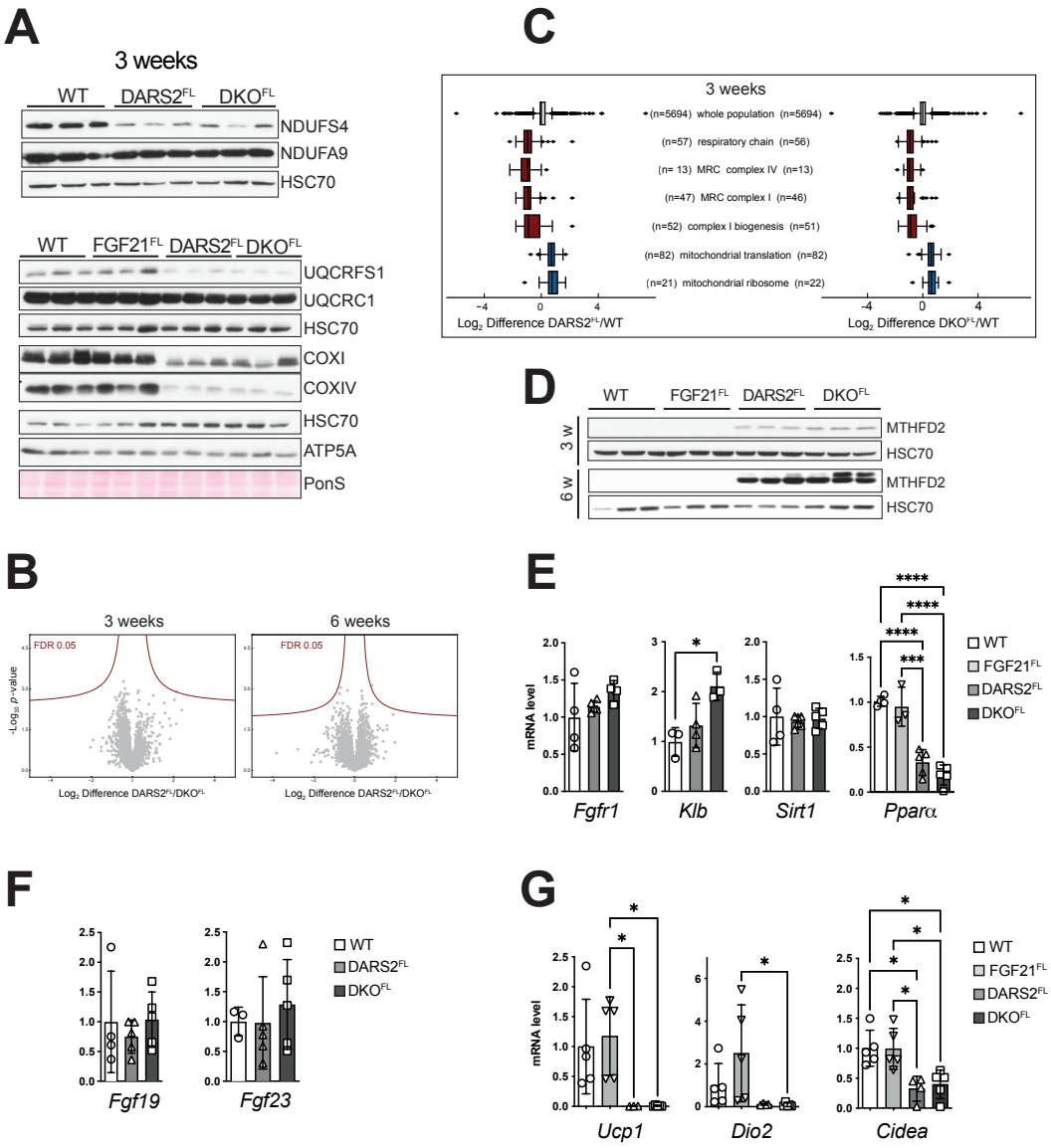
A
3 weeks
WT
DARS2FL
DKOFL
NDUFS4
NDUFA9
HSC70
WT
FGF21FL
DARS2FL
DKOFL
UQCRFS1
UQCRC1
HSC70
COXI
COXIV
HSC70
ATP5A
PonS
C
3 weeks
(n=5694) whole population (n=5694)
(n=57) respiratory chain (n=56)
(n= 13) MRC complex IV (n=13)
(n=47) MRC complex I (n=46)
(n=52) complex I biogenesis (n=51)
(n=82) mitochondrial translation (n=82)
(n=21) mitochondrial ribosome (n=22)
Log2 Difference DARS2FL/WT
Log2 Difference DKOFL/WT
D
WT
FGF21FL
DARS2FL
DKOFL
3 w
6 w
MTHFD2
HSC70
MTHFD2
HSC70
B
3 weeks
6 weeks
FDR 0.05
FDR 0.05
-Log10 p-value
Log2 Difference DARS2FL/DKOFL
Log2 Difference DARS2FL/DKOFL
E
mRNA level
Fgfr1
Klb
Sirt1
Pparα
WT
FGF21FL
DARS2FL
DKOFL
F
Fgf19
Fgf23
WT
DARS2FL
DKOFL
G
mRNA level
Ucp1
Dio2
Cidea
WT
FGF21FL
DARS2FL
DKOFL

Figure S2. Overall changes in DARS2 were not altered upon tissue-specific FGF21 loss both in earlier and later stage.

(A) Western blot analyses of individual OXPHOS subunits in 3-week-old heart lysates. Antibodies used were raised against proteins indicated in panels. HSC70 and PonS were used as a loading control (n=3). (B) Volcano plots of whole heart proteome comparing changes between DKO^{FL} and $DARS2^{FL}$ at 3 (left) and 6 weeks of age (right). (C) 1D enrichment pathway analysis showing commonly enriched pathways between $DARS^{FL}$/WT and DKO^{FL}/WT. Data are represented as the mean values +- 95% confidence interval (CI). (n= number of specific proteins identified in listed GO terms). (D) Western blot analyses of MTHFD2 levels in heart lysates at 3 and 6 weeks of age. HSC70 was used as a loading control (n=3). (E-F) Relative transcript levels of designated genes involved in FGF21 signaling or (G) adipose tissue browning determined by RT-qPCR (n=3-5). Bars represent mean ± SD (one-way ANOVA and Tukey's multiple comparisons test, *$p<0.05$, ***$p<0.001$, ****$p<0.0001$).

Figure S3

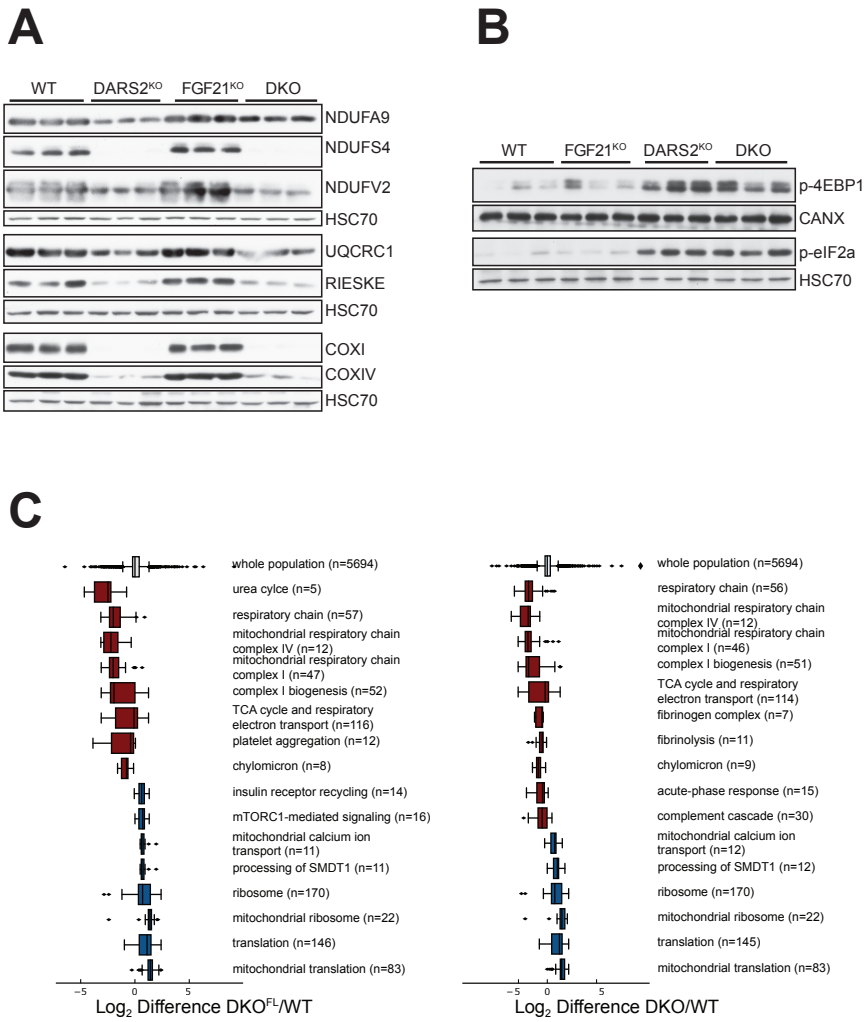
A
WT
DARS2KO
FGF21KO
DKO
NDUFA9
NDUFS4
NDUFV2
HSC70
UQCRC1
RIESKE
HSC70
COXI
COXIV
HSC70
B
WT
FGF21KO
DARS2KO
DKO
p-4EBP1
CANX
p-eIF2a
HSC70
C
whole population (n=5694)
urea cylce (n=5)
respiratory chain (n=57)
mitochondrial respiratory chain complex IV (n=12)
mitochondrial respiratory chain complex I (n=47)
complex I biogenesis (n=52)
TCA cycle and respiratory electron transport (n=116)
platelet aggregation (n=12)
chylomicron (n=8)
insulin receptor recycling (n=14)
mTORC1-mediated signaling (n=16)
mitochondrial calcium ion transport (n=11)
processing of SMDT1 (n=11)
ribosome (n=170)
mitochondrial ribosome (n=22)
translation (n=146)
mitochondrial translation (n=83)
−5
0
5
Log2 Difference DKOFL/WT
whole population (n=5694)
respiratory chain (n=56)
mitochondrial respiratory chain complex IV (n=12)
mitochondrial respiratory chain complex I (n=46)
complex I biogenesis (n=51)
TCA cycle and respiratory electron transport (n=114)
fibrinogen complex (n=7)
fibrinolysis (n=11)
chylomicron (n=9)
acute-phase response (n=15)
complement cascade (n=30)
mitochondrial calcium ion transport (n=12)
processing of SMDT1 (n=12)
ribosome (n=170)
mitochondrial ribosome (n=22)
translation (n=145)
mitochondrial translation (n=83)
−5
0
5
Log2 Difference DKO/WT

Figure S3. Full-body FGF21 depletion in DARS2 KO does not lead to changes in molecular phenotype.

(A-B) Western blot analyses of different OXPHOS proteins (A) and phosphorylated forms of 4E-BP1 and eIF2α (B) in heart lysates from WT, $FGF21^{KO}$, $DARS2^{KO}$ and DKO at 6 weeks of age. Antibodies used were raised against proteins indicated in panels. HSC70 and CANX were used as loading controls (n=3). (C) 1D enrichment analyses showing enriched pathways in tissue-specific DKO^{FL} (*left*) and DKO (*right*) relative to WT. Data are represented as the mean values +- 95% confidence interval (CI). (n = number of specific proteins identified in listed GO terms).

Figure S4

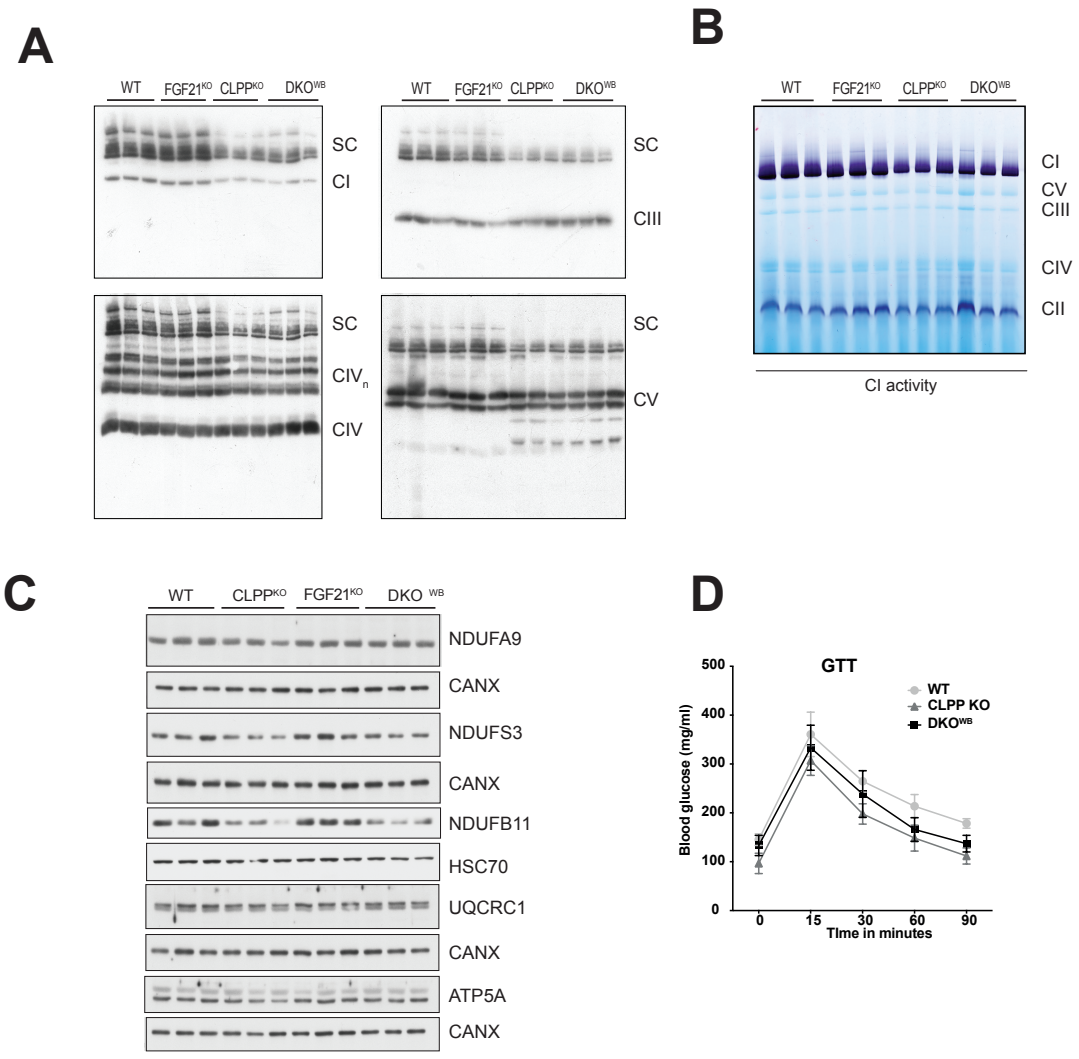
A
WT
FGF21KO
CLPPKO
DKOWB
SC
CI
CIII
CIVn
CIV
CV
B
CI
CV
CIII
CIV
CII
CI activity
C
NDUFA9
CANX
NDUFS3
NDUFB11
HSC70
UQCRC1
ATP5A
D
GTT
WT
CLPP KO
DKOWB
Blood glucose (mg/ml)
Time in minutes

Figure S4: OXPHOS is not additionally affected upon FGF21 depletion in CLPP KO mice. (A) Blue native polyacrylamide gel electrophoresis (BN-PAGE) in the presence of digitonin and subsequent western blot analysis of OXPHOS complexes and supercomplexes in mitochondria isolated from WT, FGF21 KO, CLPP KO and DKO^{WB} animals. The membranes were incubated with antibodies raised against NDUFA9 (CI), COXI (CIV), UQCRC1 (CIII) and ATP5A (CV) (*n* = 3). (B) Complex I in-gel activity of heart mitochondria in the presence of n-Dodecyl-B-D-Maltoside (DDM) at 17 weeks of age (n=3). (C) Western blot analyses of OXPHOS subunits in total heart lysates of older mice (60-70 weeks of age). Antibodies used were raised against proteins indicated in panels. HSC70 and CANX were used as loading controls (n=3). (D) Glucose tolerance tests were carried out in 15-week-old animals following a six hours fast. Blood glucose levels were determined at 15, 30, 60 and 90 min post-glucose injection.

Figure S5

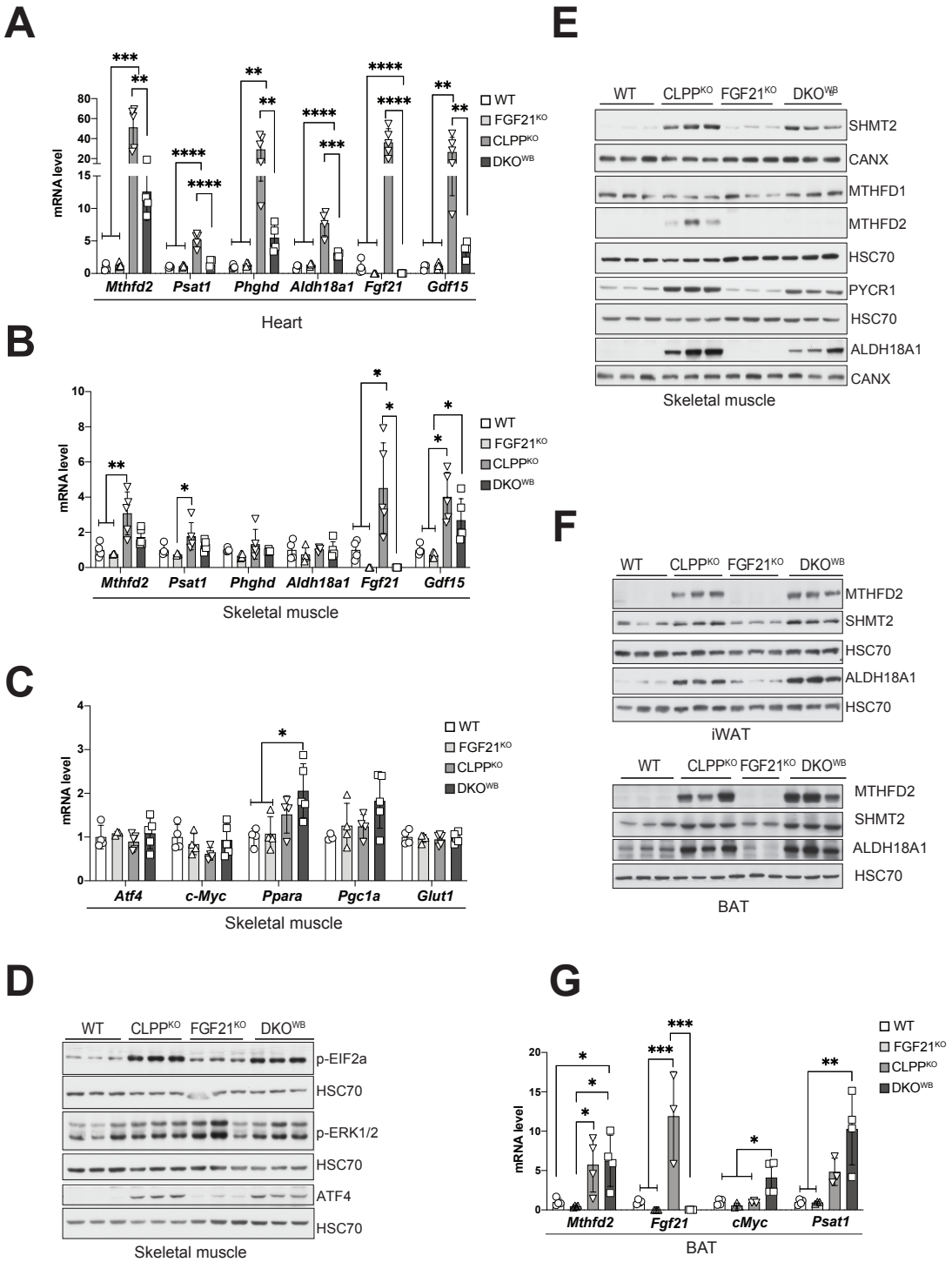
A
mRNA level
WT
FGF21KO
CLPPKO
DKOWB
Mthfd2
Psat1
Phghd
Aldh18a1
Fgf21
Gdf15
Heart
B
Skeletal muscle
C
Atf4
c-Myc
Ppara
Pgc1a
Glut1
Skeletal muscle
D
p-EIF2a
HSC70
p-ERK1/2
HSC70
ATF4
HSC70
Skeletal muscle
E
SHMT2
CANX
MTHFD1
MTHFD2
HSC70
PYCR1
HSC70
ALDH18A1
CANX
Skeletal muscle
F
MTHFD2
SHMT2
HSC70
ALDH18A1
HSC70
iWAT
MTHFD2
SHMT2
ALDH18A1
HSC70
BAT
G
Mthfd2
Fgf21
cMyc
Psat1
BAT

Figure S5: One-carbon-metabolism is changed predominantly in cardiomyocytes upon FGF21 depletion in CLPP KO mice.

(A-C) Relative transcript levels of selected genes in heart (A) or skeletal muscle (B-C) determined by RT-qPCR (n=3-5).). (D-G) Western blot analyses of (D-E) skeletal muscle, (F) iWAT and BAT protein lysates from WT, $FGF21^{KO}$, $CLPP^{KO}$ and DKO at 17 weeks of age. Antibodies used were raised against proteins indicated in panels. HSC70 and CANX were used as loading controls (n=3). (G) Relative transcript levels of selected genes in BAT determined by RT-qPCR (n=3-5). (A-C, G) Bars represent mean ± SD (one-way ANOVA and Tukey's multiple comparisons test, *p<0.05, **p<0.01, ***p<0.001, ****p<0.0001).

Supplemental Tables:

Table S1. Label-free quantification of the cardiac proteome in WT, FGF21^{FL}, DARS2 KO and DKO^{FL} at 3 weeks of age.

Table S2. Label-free quantification of the cardiac proteome in WT, FGF21^{FL}, DARS2 KO and DKO^{FL} at 6 weeks of age.

Table S3. Label-free quantification of the cardiac proteome in WT, FGF21^{KO}, DARS2 KO and DKO at 6 weeks of age.

Table S4. Global changes in the transcriptome in FGF21 KO, CLPP KO and DKO^{WB} vs. control hearts.

Table S5. GO Term and KEGG pathway analyses of transcriptome changes in FGF21 KO, CLPP KO and DKO^{WB} vs. control hearts.

Table S6. Label-free quantification of the cardiac proteome with all significant changes (FDR<0.05) between DKO and CLPP KO mice at 16 weeks of age.

Table S7 GO Term and KEGG pathway analyses of changes in proteome in FGF21 KO, CLPP KO and DKO^{WB} vs. control hearts.

REFERENCES AND NOTES

1. X. R. Bao, S. E. Ong, O. Goldberger, J. Peng, R. Sharma, D. A. Thompson, S. B. Vafai, A. G. Cox, E. Marutani, F. Ichinose, W. Goessling, A. Regev, S. A. Carr, C. B. Clish, V. K. Mootha, Mitochondrial dysfunction remodels one-carbon metabolism in human cells. *eLife* **5**, e10575 (2016).

2. P. M. Quiros, M. A. Prado, N. Zamboni, D. D'Amico, R. W. Williams, D. Finley, S. P. Gygi, J. Auwerx, Multi-omics analysis identifies ATF4 as a key regulator of the mitochondrial stress response in mammals. *J. Cell Biol.* **216**, 2027–2045 (2017).

3. M. Costa-Mattioli, P. Walter, The integrated stress response: From mechanism to disease. *Science* **368**, eaat5314 (2020).

4. E. Fessler, E. M. Eckl, S. Schmitt, I. A. Mancilla, M. F. Meyer-Bender, M. Hanf, J. Philippou-Massier, S. Krebs, H. Zischka, L. T. Jae, A pathway coordinated by DELE1 relays mitochondrial stress to the cytosol. *Nature* **579**, 433–437 (2020).

5. X. Guo, G. Aviles, Y. Liu, R. Tian, B. A. Unger, Y. T. Lin, A. P. Wiita, K. Xu, M. A. Correia, M. Kampmann, Mitochondrial stress is relayed to the cytosol by an OMA1-DELE1-HRI pathway. *Nature* **579**, 427–432 (2020).

6. H. Tyynismaa, C. J. Carroll, N. Raimundo, S. Ahola-Erkkila, T. Wenz, H. Ruhanen, K. Guse, A. Hemminki, K. E. Peltola-Mjosund, V. Tulkki, M. Oresic, C. T. Moraes, K. Pietilainen, I. Hovatta, A. Suomalainen, Mitochondrial myopathy induces a starvation-like response. *Hum. Mol. Genet.* **19**, 3948–3958 (2010).

7. S. Yatsuga, Y. Fujita, A. Ishii, Y. Fukumoto, H. Arahata, T. Kakuma, T. Kojima, M. Ito, M. Tanaka, R. Saiki, Y. Koga, Growth differentiation factor 15 as a useful biomarker for mitochondrial disorders. *Ann. Neurol.* **78**, 814–823 (2015).

8. N. A. Khan, J. Nikkanen, S. Yatsuga, C. Jackson, L. Wang, S. Pradhan, R. Kivela, A. Pessia, V. Velagapudi, A. Suomalainen, mTORC1 regulates mitochondrial integrated stress response and mitochondrial myopathy progression. *Cell Metab.* **26**, 419–428.e415 (2017).

9. M. J. Potthoff, S. A. Kliewer, D. J. Mangelsdorf, Endocrine fibroblast growth factors 15/19 and 21: From feast to famine. *Genes Dev.* **26**, 312–324 (2012).

10. P. K. Fazeli, M. Lun, S. M. Kim, M. A. Bredella, S. Wright, Y. Zhang, H. Lee, C. Catana, A. Klibanski, P. Patwari, M. L. Steinhauser, FGF21 and the late adaptive response to starvation in humans. *J. Clin. Invest.* **125**, 4601–4611 (2015).

11. S. A. Dogan, C. Pujol, P. Maiti, A. Kukat, S. Wang, S. Hermans, K. Senft, R. Wibom, E. I. Rugarli, A. Trifunovic, Tissue-specific loss of DARS2 activates stress responses independently of respiratory chain deficiency in the heart. *Cell Metab.* **19**, 458–469 (2014).

12. L. M. Restelli, B. Oettinghaus, M. Halliday, C. Agca, M. Licci, L. Sironi, C. Savoia, J. Hench, M. Tolnay, A. Neutzner, A. Schmidt, A. Eckert, G. Mallucci, L. Scorrano, S. Frank, Neuronal mitochondrial dysfunction activates the integrated stress response to induce fibroblast growth factor 21. *Cell Rep.* **24**, 1407–1414 (2018).

13. C. Becker, A. Kukat, K. Szczepanowska, S. Hermans, K. Senft, C. P. Brandscheid, P. Maiti, A. Trifunovic, CLPP deficiency protects against metabolic syndrome but hinders adaptive thermogenesis. *EMBO Rep.* **19**, e45126 (2018).

14. A. Kukat, S. A. Dogan, D. Edgar, A. Mourier, C. Jacoby, P. Maiti, J. Mauer, C. Becker, K. Senft, R. Wibom, A. P. Kudin, K. Hultenby, U. Flogel, S. Rosenkranz, D. Ricquier, W. S. Kunz, A. Trifunovic, Loss of UCP2 attenuates mitochondrial dysfunction without altering ROS production and uncoupling activity. *PLOS Genet.* **10**, e1004385 (2014).

15. R. O. Pereira, S. M. Tadinada, F. M. Zasadny, K. J. Oliveira, K. M. P. Pires, A. Olvera, J. Jeffers, R. Souvenir, R. McGlauflin, A. Seei, T. Funari, H. Sesaki, M. J. Potthoff, C. M. Adams, E. J. Anderson, E. D. Abel, OPA1 deficiency promotes secretion of FGF21 from muscle that prevents obesity and insulin resistance. *EMBO J.* **36**, 2126–2145 (2017).

16. A. Planavila, I. Redondo, E. Hondares, M. Vinciguerra, C. Munts, R. Iglesias, L. A. Gabrielli, M. Sitges, M. Giralt, M. van Bilsen, F. Villarroya, Fibroblast growth factor 21 protects against cardiac hypertrophy in mice. *Nat. Commun.* **4**, 2019 (2013).

17. S. Kaspar, C. Oertlin, K. Szczepanowska, A. Kukat, K. Senft, C. Lucas, S. Brodesser, M. Hatzoglou, O. Larsson, I. Topisirovic, A. Trifunovic, Adaptation to mitochondrial stress requires CHOP-directed tuning of ISR. *Sci. Adv.* **7**, eabf0971 (2021).

18. G. Y. Liu, D. M. Sabatini, mTOR at the nexus of nutrition, growth, ageing and disease. *Nat. Rev. Mol. Cell Biol.* **21**, 183–203 (2020).

19. C. Degirolamo, C. Sabba, A. Moschetta, Therapeutic potential of the endocrine fibroblast growth factors FGF19, FGF21 and FGF23. *Nat. Rev. Drug Discov.* **15**, 51–69 (2016).

20. A. Planavila, I. Redondo-Angulo, F. Villarroya, FGF21 and cardiac physiopathology. *Front. Endocrinol.* **6**, 133 (2015).

21. F. M. Fisher, S. Kleiner, N. Douris, E. C. Fox, R. J. Mepani, F. Verdeguer, J. Wu, A. Kharitonenkov, J. S. Flier, E. Maratos-Flier, B. M. Spiegelman, FGF21 regulates PGC-1α and browning of white adipose tissues in adaptive thermogenesis. *Genes Dev.* **26**, 271–281 (2012).

22. K. Szczepanowska, P. Maiti, A. Kukat, E. Hofsetz, H. Nolte, K. Senft, C. Becker, B. Ruzzenente, H. T. Hornig-Do, R. Wibom, R. J. Wiesner, M. Kruger, A. Trifunovic, CLPP coordinates mitoribosomal assembly through the regulation of ERAL1 levels. *EMBO J.* **35**, 2566–2583 (2016).

23. K. Szczepanowska, K. Senft, J. Heidler, M. Herholz, A. Kukat, M. N. Hohne, E. Hofsetz, C. Becker, S. Kaspar, H. Giese, K. Zwicker, S. Guerrero-Castillo, L. Baumann, J. Kauppila, A. Rumyantseva, S. Muller, C. K. Frese, U. Brandt, J. Riemer, I. Wittig, A. Trifunovic, A salvage pathway maintains highly functional respiratory complex I. *Nat. Commun.* **11**, 1643 (2020).

24. M. K. Badman, A. Koester, J. S. Flier, A. Kharitonenkov, E. Maratos-Flier, Fibroblast growth factor 21-deficient mice demonstrate impaired adaptation to ketosis. *Endocrinology* **150**, 4931–4940 (2009).

25. D. W. Huang, B. T. Sherman, R. A. Lempicki, Systematic and integrative analysis of large gene lists using DAVID bioinformatics resources. *Nat. Protoc.* **4**, 44–57 (2009).

26. A. Bruhat, J. Averous, V. Carraro, C. Zhong, A. M. Reimold, M. S. Kilberg, P. Fafournoux, Differences in the molecular mechanisms involved in the transcriptional activation of the CHOP and asparagine synthetase genes in response to amino acid deprivation or activation of the unfolded protein response. *J. Biol. Chem.* **277**, 48107–48114 (2002).

27. S. Forsstrom, C. B. Jackson, C. J. Carroll, M. Kuronen, E. Pirinen, S. Pradhan, A. Marmyleva, M. Auranen, I. M. Kleine, N. A. Khan, A. Roivainen, P. Marjamaki, H. Liljenback, L. Wang, B. J. Battersby, U. Richter, V. Velagapudi, J. Nikkanen, L. Euro, A. Suomalainen, Fibroblast growth factor 21 drives dynamics of local and systemic stress responses in mitochondrial myopathy with mtDNA deletions. *Cell Metab.* **30**, 1040–1054.e1047 (2019).

28. F. Siu, P. J. Bain, R. LeBlanc-Chaffin, H. Chen, M. S. Kilberg, ATF4 is a mediator of the nutrient-sensing response pathway that activates the human asparagine synthetase gene. *J. Biol. Chem.* **277**, 24120–24127 (2002).

29. F. Siu, C. Chen, C. Zhong, M. S. Kilberg, CCAAT/enhancer-binding protein-beta is a mediator of the nutrient-sensing response pathway that activates the human asparagine synthetase gene. *J. Biol. Chem.* **276**, 48100–48107 (2001).

30. I. Kuhl, M. Miranda, I. Atanassov, I. Kuznetsova, Y. Hinze, A. Mourier, A. Filipovska, N. G. Larsson, Transcriptomic and proteomic landscape of mitochondrial dysfunction reveals secondary coenzyme Q deficiency in mammals. *eLife* **6**, e30952 (2017).

31. A. D. Rouillard, G. W. Gundersen, N. F. Fernandez, Z. Wang, C. D. Monteiro, M. G. McDermott, A. Ma'ayan, The harmonizome: A collection of processed datasets gathered to serve and mine knowledge about genes and proteins. *Database* **2016**, baw100 (2016).

32. M. J. Li, Z. Liu, P. Wang, M. P. Wong, M. R. Nelson, J. P. Kocher, M. Yeager, P. C. Sham, S. J. Chanock, Z. Xia, J. Wang, GWASdb v2: An update database for human genetic variants identified by genome-wide association studies. *Nucleic Acids Res.* **44**, D869–D876 (2016).

33. S. Pletscher-Frankild, A. Palleja, K. Tsafou, J. X. Binder, L. J. Jensen, DISEASES: Text mining and data integration of disease-gene associations. *Methods* **74**, 83–89 (2015).

34. P. H. Sugden, A. Clerk, Regulation of the ERK subgroup of MAP kinase cascades through G protein-coupled receptors. *Cell. Signal.* **9**, 337–351 (1997).

35. O. F. Bueno, J. D. Molkentin, Involvement of extracellular signal-regulated kinases 1/2 in cardiac hypertrophy and cell death. *Circ. Res.* **91**, 776–781 (2002).

36. U. Kintscher, A. Foryst-Ludwig, G. Haemmerle, R. Zechner, The role of adipose triglyceride lipase and cytosolic lipolysis in cardiac function and heart failure. *Cell Rep. Med.* **1**, 100001 (2020).

37. K. H. Kim, Y. T. Jeong, H. Oh, S. H. Kim, J. M. Cho, Y. N. Kim, S. S. Kim, D. H. Kim, K. Y. Hur, H. K. Kim, T. Ko, J. Han, H. L. Kim, J. Kim, S. H. Back, M. Komatsu, H. Chen, D. C. Chan, M. Konishi, N. Itoh, C. S. Choi, M. S. Lee, Autophagy deficiency leads to protection from obesity and insulin resistance by inducing Fgf21 as a mitokine. *Nat. Med.* **19**, 83–92 (2013).

38. A. Salminen, K. Kaarniranta, A. Kauppinen, Integrated stress response stimulates FGF21 expression: Systemic enhancer of longevity. *Cell. Signal.* **40**, 10–21 (2017).

39. J. Nikkanen, S. Forsstrom, L. Euro, I. Paetau, R. A. Kohnz, L. Wang, D. Chilov, J. Viinamaki, A. Roivainen, P. Marjamaki, H. Liljenback, S. Ahola, J. Buzkova, M. Terzioglu, N. A. Khan, S. Pirnes-Karhu, A. Paetau, T. Lonnqvist, A. Sajantila, P. Isohanni, H. Tyynismaa, D. K. Nomura, B. J. Battersby, V. Velagapudi, C. J. Carroll, A. Suomalainen, Mitochondrial DNA replication defects disturb cellular dntp pools and remodel one-carbon metabolism. *Cell Metab.* **23**, 635–648 (2016).

40. J. Shan, F. Zhang, J. Sharkey, T. A. Tang, T. Ord, M. S. Kilberg, The C/ebp-Atf response element (CARE) location reveals two distinct Atf4-dependent, elongation-mediated mechanisms for transcriptional induction of aminoacyl-tRNA synthetase genes in response to amino acid limitation. *Nucleic Acids Res.* **44**, 9719–9732 (2016).

41. M. A. Nikiforov, S. Chandriani, B. O'Connell, O. Petrenko, I. Kotenko, A. Beavis, J. M. Sedivy, M. D. Cole, A functional screen for Myc-responsive genes reveals serine hydroxymethyltransferase, a major source of the one-carbon unit for cell metabolism. *Mol. Cell. Biol.* **22**, 5793–5800 (2002).

42. H. Q. Ju, Y. X. Lu, D. L. Chen, Z. X. Zuo, Z. X. Liu, Q. N. Wu, H. Y. Mo, Z. X. Wang, D. S. Wang, H. Y. Pu, Z. L. Zeng, B. Li, D. Xie, P. Huang, M. C. Hung, P. J. Chiao, R. H. Xu, Modulation of

redox homeostasis by inhibition of MTHFD2 in colorectal cancer: Mechanisms and therapeutic implications. *J. Natl. Cancer Inst.* **111**, 584–596 (2019).

43. S. C. Johnson, M. E. Yanos, E. B. Kayser, A. Quintana, M. Sangesland, A. Castanza, L. Uhde, J. Hui, V. Z. Wall, A. Gagnidze, K. Oh, B. M. Wasko, F. J. Ramos, R. D. Palmiter, P. S. Rabinovitch, P. G. Morgan, M. M. Sedensky, M. Kaeberlein, mTOR inhibition alleviates mitochondrial disease in a mouse model of Leigh syndrome. *Science* **342**, 1524–1528 (2013).

44. G. Civiletto, S. A. Dogan, R. Cerutti, G. Fagiolari, M. Moggio, C. Lamperti, C. Beninca, C. Viscomi, M. Zeviani, Rapamycin rescues mitochondrial myopathy via coordinated activation of autophagy and lysosomal biogenesis. *EMBO Mol. Med.* **10**, e8799 (2018).

45. O. Ignatenko, J. Nikkanen, A. Kononov, N. Zamboni, G. Ince-Dunn, A. Suomalainen, Mitochondrial spongiotic brain disease: Astrocytic stress and harmful rapamycin and ketosis effect. *Life Sci. Alliance* **3**, e202000797 (2020).

46. K. L. Perks, G. Rossetti, I. Kuznetsova, L. A. Hughes, J. A. Ermer, N. Ferreira, J. D. Busch, D. L. Rudler, H. Spahr, T. Schondorf, A. J. Shearwood, H. M. Viola, S. J. Siira, L. C. Hool, D. Milenkovic, N. G. Larsson, O. Rackham, A. Filipovska, PTCD1 is required for 16S rRNA maturation complex stability and mitochondrial ribosome assembly. *Cell Rep.* **23**, 127–142 (2018).

47. K. L. Perks, N. Ferreira, T. R. Richman, J. A. Ermer, I. Kuznetsova, A. J. Shearwood, R. G. Lee, H. M. Viola, V. P. A. Johnstone, V. Matthews, L. C. Hool, O. Rackham, A. Filipovska, Adult-onset obesity is triggered by impaired mitochondrial gene expression. *Sci. Adv.* **3**, e1700677 (2017).

48. J. van der Velden, G. J. M. Stienen, Cardiac disorders and pathophysiology of sarcomeric proteins. *Physiol. Rev.* **99**, 381–426 (2019).

49. V. Szuts, D. Menesi, Z. Varga-Orvos, A. Zvara, N. Houshmand, M. Bitay, G. Bogats, L. Virag, I. Baczko, B. Szalontai, A. Geramipoor, D. Cotella, E. Wettwer, U. Ravens, F. Deak, L. G. Puskas, J. G. Papp, I. Kiss, A. Varro, N. Jost, Altered expression of genes for Kir ion channels in dilated cardiomyopathy. *Can. J. Physiol. Pharmacol.* **91**, 648–656 (2013).

50. L. U. Magnusson, A. Lundqvist, J. Asp, J. Synnergren, C. T. Johansson, L. Palmqvist, A. Jeppsson, L. M. Hulten, High expression of arachidonate 15-lipoxygenase and proinflammatory markers in human ischemic heart tissue. *Biochem. Biophys. Res. Commun.* **424**, 327–330 (2012).

51. S. A. Mahmoud, C. Poizat, Epigenetics and chromatin remodeling in adult cardiomyopathy. *J. Pathol.* **231**, 147–157 (2013).

52. H. Zhang, Z. Yu, J. He, B. Hua, G. Zhang, Identification of the molecular mechanisms underlying dilated cardiomyopathy via bioinformatic analysis of gene expression profiles. *Exp. Ther. Med.* **13**, 273–279 (2017).

53. G. W. Dorn II, R. B. Vega, D. P. Kelly, Mitochondrial biogenesis and dynamics in the developing and diseased heart. *Genes Dev.* **29**, 1981–1991 (2015).

54. P. Ahuja, P. Zhao, E. Angelis, H. Ruan, P. Korge, A. Olson, Y. Wang, E. S. Jin, F. M. Jeffrey, M. Portman, W. R. Maclellan, Myc controls transcriptional regulation of cardiac metabolism and mitochondrial biogenesis in response to pathological stress in mice. *J. Clin. Invest.* **120**, 1494–1505 (2010).

55. M. Aradjanski, "The role of fibroblast growth factor 21 in different mouse models of mitochondrial dysfunction," thesis, University of Cologne, Cologne, Germany (2018).

56. N. G. Larsson, J. Wang, H. Wilhelmsson, A. Oldfors, P. Rustin, M. Lewandoski, G. S. Barsh, D. A. Clayton, Mitochondrial transcription factor A is necessary for mtDNA maintenance and embryogenesis in mice. *Nat. Genet.* **18**, 231–236 (1998).

57. M. J. Potthoff, T. Inagaki, S. Satapati, X. Ding, T. He, R. Goetz, M. Mohammadi, B. N. Finck, D. J. Mangelsdorf, S. A. Kliewer, S. C. Burgess, FGF21 induces PGC-1α and regulates carbohydrate and fatty acid metabolism during the adaptive starvation response. *Proc. Natl. Acad. Sci. U.S.A.* **106**, 10853–10858 (2009).

58. R. Janky, A. Verfaillie, H. Imrichova, B. Van de Sande, L. Standaert, V. Christiaens, G. Hulselmans, K. Herten, M. Naval Sanchez, D. Potier, D. Svetlichnyy, Z. Kalender Atak, M. Fiers, J. C. Marine,

S. Aerts, iRegulon: From a gene list to a gene regulatory network using large motif and track collections. *PLOS Comput. Biol.* **10**, e1003731 (2014).

59. S. Chen, Y. Zhou, Y. Chen, J. Gu, fastp: An ultra-fast all-in-one FASTQ preprocessor. *Bioinformatics* **34**, i884–i890 (2018).

60. N. L. Bray, H. Pimentel, P. Melsted, L. Pachter, Near-optimal probabilistic RNA-seq quantification. *Nat. Biotechnol.* **34**, 525–527 (2016).

61. M. D. Robinson, D. J. McCarthy, G. K. Smyth, edgeR: A Bioconductor package for differential expression analysis of digital gene expression data. *Bioinformatics* **26**, 139–140 (2010).

62. C. Soneson, M. I. Love, M. D. Robinson, Differential analyses for RNA-seq: Transcript-level estimates improve gene-level inferences. *F1000Res.* **4**, 1521 (2015).

63. M. I. Love, W. Huber, S. Anders, Moderated estimation of fold change and dispersion for RNA-seq data with DESeq2. *Genome Biol.* **15**, 550 (2014).